Research Square

Preprints are preliminary reports that have not undergone peer review.
They should not be considered conclusive, used to inform clinical practice,
or referenced by the media as validated information.

Symmetric material interpolation scheme without artificial stiffness reduction at material interfaces for multimaterial topology optimization

Shun Ogawa

ogawa@struct.t.u-tokyo.ac.jp

The University of Tokyo: Tokyo Daigaku https://orcid.org/0009-0006-0480-1309

Katsuyuki Suzuki

The University of Tokyo

Research Article

Keywords: Topology optimization, Multimaterial, Discrete Material Optimization, Material interpolation, Density filter

Posted Date: November 26th, 2026

DOI: https://doi.org/10.21203/rs.3.rs-11885576/v1

License: This work is licensed under a Creative Commons Attribution 4.0 International License.
Read Full License

Additional Declarations: The authors declare no competing interests.

Symmetric material interpolation scheme without artificial stiffness reduction at material interfaces for multimaterial topology optimization

Shun Ogawa[1*] and Katsuyuki Suzuki[1]

[1*]Department of Systems Innovation, The University of Tokyo, 7-3-1, Hongo, Bunkyo-ku, 113-8656, Tokyo, Japan.

*Corresponding author(s). E-mail(s): ogawa@struct.t.u-tokyo.ac.jp;

Abstract

This study proposes solid–composition material interpolation (SCMI), a material interpolation scheme for multimaterial topology optimization. SCMI consists of a mapping that converts design variables into volume fractions before filtering, separate application of Heaviside projection to the solid amount and the composition, and a mixture rule that gives the Young's modulus value of the solid part as a composition-weighted power mean of the material moduli. Because this scheme treats all materials using expressions of the same form, the optimization result does not depend on the order of material definition. In addition, owing to the mapping, the sum of the material volume fractions at each location is kept at or below unity without imposing additional constraints, and Young's modulus at an interface filled with materials lies between the moduli of the materials on both sides. Therefore, while retaining the symmetry of material definition under discrete material optimization (DMO), SCMI avoids the artificial stiffness reduction at material interfaces, which arises when DMO is combined with a density filter and which depends on numerical parameters, such as the penalty exponent and filter radius. For gradient-based optimization, the sensitivity of the objective function to the design variables is formulated via the adjoint variable method and verified against that determined using the finite difference method. Numerical examples show that SCMI yields mechanically reasonable optimal structures without artificial stiffness reduction at material interfaces, regardless of the order of material definition.

Keywords: Topology optimization, Multimaterial, Discrete Material Optimization, Material interpolation, Density filter

1 Introduction

Multimaterial design, which combines several materials with different properties, has attracted attention as a means of further improving the performance of mechanical structures. Compared with single-material design, multimaterial design has a much higher degree of design freedom, covering not only structural layouts but also material types and their arrangements, which introduces difficulties into deriving an optimal structure that satisfies the required specifications. Multimaterial topology optimization, which extends topology optimization[1] to multiple materials, has been actively studied to address this problem.

Structural representation for handling multiple materials, that is, interpolation from design variables to material properties, has long been discussed in multimaterial topology optimization. The representative density-based method solid isotropic material with penalization (SIMP) [1–3] has been extended to three-phase materials. In this method, the first design variable represents the presence of solid, and the second and subsequent design variables determine the material assigned to each part of the structure, according to a fixed order; hence, $m - 1$ types of design variables must be defined for m material phases, and the number of design variables increases with the number of materials considered. In addition, a change in the order of the material properties assigned to the design variables produces different optimization results, even for problems that should normally give the same result. Methods that represent multiple materials with a single type of design variable have been proposed to address the increase in the number of design variables, such as peak function material interpolation[4], which extracts a material using a normal distribution function that approximates the δ function, and ordered SIMP[5], which introduces normalized design variables. An advantage of ordered SIMP is that the number of design variables does not depend on the number of materials. However, the design variables of individual materials are not independent, and the materials must be sorted in order of their normalized densities. Moreover, da Silveira and Palma[6] reported that the interpolation function of ordered SIMP does not penalize intermediate densities in the intervals between solid materials. Other methods that use a single type of design variable map it to the variables of individual materials[7, 8]. Swan and Kosaka[9] proposed an early method that interpolates material properties using the Voigt and Reuss mixture rules. Tavakoli and Mohseni[10] proposed the alternating active-phase algorithm, which decomposes a multimaterial problem into a sequence of two-phase subproblems and solves them using a block coordinate descent method similar to the Gauss–Seidel method. This method uses a weighted sum with powers of the phases' volume fractions for the interpolation of material properties and can use existing two-phase optimization methods to solve the subproblems; hence, it is easily extended to many materials. However, because this Gauss–Seidel-type algorithm solves the two-phase subproblems sequentially in a fixed order, the result depends on the material order. Thus, many methods have drawbacks concerning the independence of the design variables and the dependence of the optimization result on the order of material definition.

Discrete material optimization (DMO)[11] resolves the above issues regarding the independence of the design variables and the symmetry of material definition. DMO sets a design variable per candidate material and expresses the constitutive law as

a weighted sum of the constitutive laws of these candidate materials. Each weight is given by the product of the design variable of the material itself and those of the other materials, and all candidate materials are treated in the same form; hence, the same optimization result is obtained regardless of the order of material definition. Noda et al.[12] proposed an extended level-set method that considers the complete symmetry of material definition. DMO has been applied to the fiber orientation and material selection of laminated composites[11, 13, 14] and to problems where many material properties must be considered and material superiority cannot be determined in general, such as transient heat conduction problems[15] and transient response problems of viscoelastic bodies[16]. The weight of each material contains terms involving the design variables of the other materials. These terms were introduced so that an increase in the weight of one material decreases the weights of the other materials, thereby promoting discrete material selection per element[11]. Thus, the sum of these weights is not unity except when the design variables have converged to 0 or 1, and a weight corresponding to void remains in mixed states where several design variables assume intermediate values. A method that normalizes these weights by their sum was presented together with DMO to address this problem; however, the authors also explain that normalization weakens the effect of pushing the design variables toward 0 or 1[11]; the same point was then presented by Bruyneel[17].

Methods other than DMO that express material properties as a weighted sum of the properties of the candidate materials have also been proposed. Gao and Zhang[18] generalized the concept of DMO to the topology optimization of structures and presented a formulation combined with mass constraints. Bruyneel[17] proposed the shape functions with penalization scheme, which uses the shape functions of a finite element as the weights, as an alternative to DMO. Yi et al.[19] proposed interpolation based on a mapping that uses the ratio of the p-norm to the 1-norm of the design variables. As in DMO, the sum of the weights in these methods is not unity in mixed states.

Methods that keep the sum of the material amounts at or below unity have also been proposed. At each design point, Hvejsel and Lund[20] imposed linear constraints that keep the sum of the design variables of the materials equal to or less than unity and proposed interpolations that generalize SIMP and rational approximation of material properties to multiple materials under these constraints. Kennedy and Martins[21] used similar linear constraints. Some methods use variable definitions to keep the sum of material amounts at unity without additional constraints. Sarkar et al.[22] used the natural coordinates of generalized shape functions defined on a hypercube as the design variables and associated the hypercube vertices with the candidate materials. Zhou et al.[23] used component memberships, or the fractions by which each design point belongs to each component, as the design variables and adopted hypercube-to-simplex projection. Chandrasekhar and Suresh[24] applied a softmax function to the output of a neural network. However, these methods also penalize material mixing by raising quantities whose sum is kept at unity to a power. This penalty is intended to avoid states in which several materials coexist in one element. Meanwhile, the filtering used to avoid the checkerboard phenomenon produces mixed states at the interfaces between different materials. Hence, this penalty also acts on interfaces.

In density-based topology optimization, a density filter[25, 26] is commonly combined with a projection using a function that approximates the Heaviside function[27]. However, when DMO is applied to the filtered design variables, stiffness decreases where different materials adjoin each other. Because the density filter averages the surrounding design variables, the filtered design variables of two materials take intermediate values at their interface, and their sum remains at unity. Volume constraints classify this region as a material-filled one, whereas DMO weights, which are designed on the premise of discrete material selection per element, identify it as a part-void state. Therefore, Young's modulus at the interface becomes lower than that of the material on either side of the interface, and the optimal structure obtained by DMO presupposes that stiffness decreases at the interfaces between materials. Stiffness often decreases at actual joints as well, and this premise is qualitatively consistent with the characteristics of joints. However, this stiffness reduction is artificial: it does not reflect the properties of the joint because it originates from the interpolation scheme. Moreover, its magnitude depends not only on the combination of the penalty exponent and the material properties but also on the numerical parameters, such as the filter radius and projection sharpness. In other words, the designer cannot specify joint stiffness as a material property.

Other methods account for the properties of material interfaces. Vermaak et al.[28] proposed a method that continuously varies the interface properties in the level-set method. The method of Clausen et al.[29] includes coating layers in the topology optimization problem by accounting for the spatial gradient of the design field in the interpolation function. Jung et al.[30] used two-step filtering to consider the joint region and its stiffness in multimaterial topology optimization. Differing in nature from the stiffness reduction caused by DMO weights, these methods deliberately model interface properties and behavior. Such deliberate assignment of interface properties requires an interpolation scheme that does not artificially reduce the stiffness at interfaces. Although extended SIMP preserves the stiffness at interfaces, it loses the symmetry of material definition. DMO and similar methods maintain the symmetry of material definition, but the sum of the weights is not unity in mixed states, and the stiffness at interfaces decreases. Methods that impose linear constraints on the sum of the design variables[20, 21] can keep the sum of the material amounts at or below unity, but the number of constraints increases with the number of design points. A method that aggregates the constraints preventing overfilling[31] initially limits the number of constraints but ultimately requires additional ones. As for methods that keep the sum at unity without additional constraints[22–24], the penalty imposed by the power also acts on the mixed states at interfaces. Thus, to the best of the authors' knowledge, no interpolation scheme maintains the symmetry of material definition, does not reduce the stiffness at interfaces, and keeps the sum of material amounts at or below unity without special constraints.

In this study, solid–composition material interpolation (SCMI) is proposed as a material interpolation scheme that satisfies these requirements simultaneously. SCMI consists of a mapping from design variables to volume fractions, Heaviside projection, and a mixture rule for material properties. This scheme has the following properties:

First, it maintains the symmetry of material definition. Because the mapping, projection, and mixture rule treat all materials using expressions of the same form, the same optimization result is obtained even when the order of material definition is changed. Second, it does not artificially decrease stiffness at the interfaces between different materials. Because the mapping is applied before filtering, the sum of the volume fractions at an interface filled with materials remains exactly unity after filtering, and no part is evaluated as void. Furthermore, the projection is applied separately to the solid amount and the composition of the filtered volume fractions, and Young's modulus in the solid part is given by a power mean weighted by the composition. Thus, Young's modulus at the interface lies between those of the materials on both sides. Third, the sum of the volume fractions of materials at the same location is kept at or below unity without additional constraints. Because the mapping defines the volume fractions of the materials and void so that they sum to unity, this property holds regardless of the values of the design variables and is preserved after filtering. The following discussion presents the SCMI formulation and shows how the above properties hold. Next, sensitivity analysis is conducted via the adjoint variable method, and its validity is confirmed through a comparison with the finite difference method. Finally, these properties are verified through several numerical examples. Findings show that SCMI does not artificially reduce stiffness at interfaces, and mechanically reasonable optimal structures are obtained regardless of the order of material definition.

2 Multimaterial topology optimization

In density-based topology optimization, the problem of finding an optimal structure is replaced by the problem of finding the optimal material distribution in a fixed design domain Ω. In a multimaterial problem, the total number of nonvoid materials is n. In this study, the design variables are defined for, and are constant within, each finite element. The design variable representing the presence of material i in element e is defined as follows:

$$0 \leq x_{ie} \leq 1 \quad (i = 1, \ldots, n;\ e = 1, \ldots, N_{\mathrm{elem}}), \tag{1}$$

where N_{elem} is the number of elements. $x_{ie} = 1$ means element e is filled with material i. Hereinafter, when the elements need not be distinguished, the subscript e is omitted and the variable is written as x_i.

A density filter[25, 26] is applied to the design variables.

$$\tilde{x}_{ie} = \frac{\sum_{j \in \mathcal{N}_e} w_{ej} V_j x_{ij}}{\sum_{j \in \mathcal{N}_e} w_{ej} V_j}, \tag{2}$$

$$w_{ej} = R - \|\boldsymbol{c}_e - \boldsymbol{c}_j\|. \tag{3}$$

$\tilde{x}_{ie}$ is the filtered design variable of element e, w_{ej} is the weight of element j for element e, $\boldsymbol{c}_e$ is the center of element e, V_j is the volume of element j, R is the filter radius, and $\mathcal{N}_e$ is the set of elements whose centers are located at a distance of less than R from the center of element e. Because the density filter averages the surrounding

design variables, grayscale tends to remain at the structure boundaries. Therefore, the following function[27] is introduced to promote the binarization of the structure:

$$\bar{x}_{ie} = H(\tilde{x}_{ie}), \tag{4}$$

$$H(a) = \frac{\tanh(\beta\eta) + \tanh(\beta(a-\eta))}{\tanh(\beta\eta) + \tanh(\beta(1-\eta))}, \tag{5}$$

where $\bar{x}_{ie}$ is the projected design variable, $H(a)$ is a function of the argument a that approximates the Heaviside function, η is the projection threshold, and β is the parameter representing projection sharpness. A material interpolation scheme gives the amount m_i of material i and Young's modulus E at each location from the above variables. The expressions of m_i and E differ between DMO (Section 3), SCMI (Section 4), and extended SIMP (Appendix A).

This study assumes an isotropic linear elastic body and formulates the optimization problem as the following compliance minimization problem, with a volume constraint for each material:

$$\begin{aligned} \min_{\boldsymbol{x}} \quad & f(\boldsymbol{x}) = \frac{1}{f_0}\boldsymbol{F}_{\mathrm{ext}}^{\mathrm{T}}\boldsymbol{U} \\ \text{subject to} \quad & \begin{cases} g_i(\boldsymbol{x}) = \dfrac{1}{|\Omega|}\displaystyle\int_\Omega m_i \,\mathrm{d}\Omega - \bar{V}_i \le 0 \quad (i = 1, \dots, n) \\ \boldsymbol{K}\boldsymbol{U} = \boldsymbol{F}_{\mathrm{ext}} \\ x_{\min} \le x_{ie} \le x_{\max} \quad (i = 1, \dots, n;\ e = 1, \dots, N_{\mathrm{elem}}), \end{cases} \end{aligned} \tag{6}$$

where f is the objective function; g_i is the constraint function on the material i volume; $|\Omega|$ is the volume of the fixed design domain; $\bar{V}_i$ is the upper limit of the volume constraint for material i; and $x_{\min}$ and $x_{\max}$ are the lower and upper bounds of the design variables, respectively. In addition, $\boldsymbol{K}$ is the global stiffness matrix, $\boldsymbol{U}$ is the global displacement vector, and $\boldsymbol{F}_{\mathrm{ext}}$ is the external force vector. f_0 is the compliance of the initial design variable distribution and is used to normalize the objective function. The global stiffness matrix $\boldsymbol{K}$ is given by the following:

$$\boldsymbol{K} = \sum_{e=1}^{N_{\mathrm{elem}}} \int_{\Omega_e} \boldsymbol{B}^{\mathrm{T}}\, \boldsymbol{C}(E)\, \boldsymbol{B} \,\mathrm{d}\Omega, \tag{7}$$

where Ω_e is the domain of element e, $\boldsymbol{B}$ is the strain–displacement matrix, and $\boldsymbol{C}(E)$ is the elasticity matrix.

3 Artificial stiffness reduction under DMO

Under DMO[11], Young's modulus is expressed as a function of the projected design variables as follows:

$$E = E_0 + \sum_{i=1}^{n} w_i(\bar{\boldsymbol{x}})\,(E_i - E_0), \tag{8}$$

$$w_i(\bar{\boldsymbol{x}}) = d(\bar{x}_i) \prod_{\substack{j=1 \\ j \neq i}}^{n} \big(1 - d(\bar{x}_j)\big), \tag{9}$$

where E_i is Young's modulus for material i, E_0 is a small Young's modulus assigned to void, w_i is the weight of material i, $d(a) = a^p$ is the penalty function, and p is the penalty exponent. Poisson's ratio is common across all materials. Because the weights are symmetric with respect to the design variables (Eq. (9)), the same optimization result is obtained even with changes in the order of the materials assigned to the design variables. The amount of material i is $m_i = \bar{x}_i$, and the volume constraints are given by Eq. (6). Hereinafter, the sum of the weights is as follows:

$$T(\bar{\boldsymbol{x}}) = \sum_{i=1}^{n} w_i(\bar{\boldsymbol{x}}). \tag{10}$$

Note that $1 - T$ corresponds to the weight assigned to void. This section shows that stiffness decreases at the interfaces between materials when DMO is applied to the filtered design variables, and explains the reduction mechanism.

As a trivial relation, $d(\bar{x}_j) + (1 - d(\bar{x}_j)) = 1$ holds for each material. The left-hand side is multiplied over all materials, the product is expanded, and the terms coinciding with the weights w_i in Eq. (9) are removed. Then, the weight of void is expressed as follows:

$$1 - T = \prod_{j=1}^{n} \big(1 - d(\bar{x}_j)\big) + \sum_{\substack{S \subseteq \{1,\dots,n\} \\ |S| \geq 2}} \prod_{j \in S} d(\bar{x}_j) \prod_{j \in \{1,\dots,n\} \setminus S} \big(1 - d(\bar{x}_j)\big), \tag{11}$$

where S is a subset of the set of material numbers $\{1, \dots, n\}$. The first term on the right-hand side corresponds to a state in which no material is selected, and the second term corresponds to a state where two or more materials overlap. Because every term on the right-hand side is nonnegative, $T < 1$ holds in all states except single-material ones.

Next, the interface between different materials is considered. Three phases are considered—consisting of void, material 1, and material 2—and the design variables are assumed binarized. In other words, $(x_1, x_2) = (1, 0)$ in the region consisting only of material 1, and $(x_1, x_2) = (0, 1)$ in the region consisting only of material 2. The two regions are assumed to adjoin each other without voids in between. In addition, the projection threshold is set to $\eta = 0.5$. In this state, $x_1 + x_2 = 1$ holds in all elements around the interface. Because the density filter (2) is a weighted average of the surrounding design variables, the sum after filtering remains unity.

$$\tilde{x}_{1e} + \tilde{x}_{2e} = \frac{\sum_{j \in \mathcal{N}_e} w_{ej} V_j \left(x_{1j} + x_{2j}\right)}{\sum_{j \in \mathcal{N}_e} w_{ej} V_j} = 1. \tag{12}$$

Furthermore, because the projection function (5) at $\eta = 0.5$ satisfies $H(1 - a) = 1 - H(a)$, the sum remains unity after the projection as well. Therefore, the design

variables at the interface take the following values:

$$(\bar{x}_1,\, \bar{x}_2) = (1-t,\, t) \quad (0 < t < 1). \tag{13}$$

In this state, the sum of the material amounts $m_i = \bar{x}_i$ is unity (Eq. (13)), and the sum of the weights is less than unity (Eq. (11)).

$$\begin{cases} m_1 + m_2 = \bar{x}_1 + \bar{x}_2 = 1 \\ T = 1 - \big(1 - d(1-t)\big)\big(1 - d(t)\big) - d(1-t)\, d(t) < 1. \end{cases} \tag{14}$$

In other words, the volume constraints (6) classify the interface as being filled with materials, whereas the stiffness identifies it as a part-void state. From Eq. (8), Young's modulus at the interface is as follows:

$$E = E_0 + d(1-t)\big(1 - d(t)\big)(E_1 - E_0) + d(t)\big(1 - d(1-t)\big)(E_2 - E_0). \tag{15}$$

Figure 1 shows Young's modulus at the interface for $E_1 = 100$ and $E_2 = 200$. Young's modulus at the interface is lower than that under a linear mixture rule and decreases as the penalty exponent p increases. For every p in Fig. 1, it becomes lower than that of the material on either side of the interface.

The amount of stiffness reduction at the interface is determined by a combination of the penalty exponent p and the material properties (Eq. (15)). Furthermore, when the design variables are constant within each element, the reduction amount depends on the filter radius and the projection sharpness parameter because the t value taken by the elements at the interface also relies on them. None of these parameters is given in the representation of the characteristics of a joint. The optimal structure obtained by DMO presupposes that stiffness decreases at the interfaces between materials, but this premise originates from the interpolation scheme, not from the joint characteristics; in other words, the stiffness reduction is artificial and cannot be controlled by the designer. To account for the stiffness reduction at a joint, the designer should provide its characteristics independently of the artificial stiffness reduction originating from the interpolation scheme.

4 Proposal of solid–composition material interpolation

Stiffness artificially reduces at interfaces because the sum of the weights does not reach unity at a material-filled interface. Normalizing the weights by their sum eliminates this reduction but weakens the penalty on material mixing[11]. Therefore, in this study, the design variables are mapped to volume fractions before filtering. Consequently, the sum of the weights at the interface remains unity, and material mixing is penalized by a nonlinear mixture rule for Young's modulus. The proposed scheme is called SCMI because it treats volume fractions separately as the solid amount and the composition. In this scheme, Young's modulus and the volume constraints are

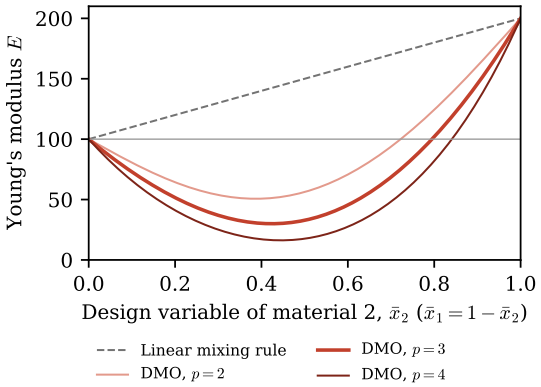


Fig. 1: Young's modulus of DMO at interface filled with material 1 ($E_1 = 100$) and material 2 ($E_2 = 200$). The horizontal axis is the design variable $\bar{x}_2$ of material 2, with $\bar{x}_1 = 1 - \bar{x}_2$. The results for the penalty exponents $p = 2, 3, 4$ and the linear mixture rule are shown.

computed from the design variables as follows:

$$\boldsymbol{x} \xrightarrow{\mathcal{M}} \boldsymbol{v} \xrightarrow{\mathcal{F}} \tilde{\boldsymbol{v}} \xrightarrow{\mathcal{P}} \bar{\boldsymbol{v}} \longrightarrow E(\bar{\boldsymbol{v}}),\ g_i(\bar{\boldsymbol{v}}), \tag{16}$$

where $\mathcal{M}$ is the elementwise mapping from the design variables $\boldsymbol{x}$ to the volume fractions $\boldsymbol{v}$, $\mathcal{F}$ is the density filter applied to each volume fraction, $\mathcal{P}$ is the projection applied separately to the solid amount and the composition, $\tilde{\boldsymbol{v}}$ denotes the filtered volume fractions, and $\bar{\boldsymbol{v}}$ denotes the projected volume fractions. Each step is described below in order.

4.1 Mapping to volume fractions

The mapping from the design variable x_i to the volume fraction v_i of material i is defined as follows:

$$\begin{cases} r_i = \dfrac{x_i}{1 - x_i} \\ v_i = \dfrac{r_i}{1 + \sum_{k=1}^{n} r_k}. \end{cases} \tag{17}$$

The volume fraction of void v_0 is defined as follows:

$$v_0 = 1 - \sum_{i=1}^{n} v_i. \tag{18}$$

Then, $r_i = v_i / v_0$ is the volume ratio of material i to void. This mapping is equivalent to treating the design variable x_i as the fraction $v_i/(v_i + v_0)$ of material i when only this material and void are considered. Multiplying the numerator and the denominator

of Eq. (17) by $\prod_{j=1}^{n}(1-x_j)$ gives the following equations:

$$\begin{cases} v_i = \dfrac{\omega_i}{\omega_0 + \sum_{k=1}^{n} \omega_k} \\ \omega_i = x_i \displaystyle\prod_{\substack{j=1 \\ j\neq i}}^{n} (1-x_j) \\ \omega_0 = \displaystyle\prod_{j=1}^{n} (1-x_j). \end{cases} \tag{19}$$

Equations (17) and (19) are the same mapping, but Eq. (19) is used in the computation. Equation (17) cannot be evaluated when a design variable is equal to 1 because it involves division by $1-x_i$. By contrast, the denominator $\omega_0 + \sum_{k=1}^{n} \omega_k$ of Eq. (19) vanishes only when two or more design variables are simultaneously equal to 1. Therefore, a small quantity $\varepsilon > 0$ is introduced, and the range of the design variables in Eq. (6) is set as follows:

$$x_{\min} \leq x_{ie} \leq 1 - \varepsilon. \tag{20}$$

Then, $\omega_0 \geq \varepsilon^n > 0$ holds, and the denominator is always positive.

The volume fractions after the mapping satisfy the following relations regardless of the values of the design variables:

$$v_i \geq 0, \qquad \sum_{i=1}^{n} v_i \leq 1. \tag{21}$$

Thus, the sum of the volume fractions of the materials in the same element does not exceed unity. The state in which only the design variable of material i is equal to 1 is mapped to $v_i = 1$, and the state in which all design variables are equal to 0 is mapped to void. In addition, the design variables and volume fractions exhibit one-to-one correspondence, and the Jacobian of the mapping is nonsingular. Therefore, the mapping does not restrict the material distributions that can be represented, and sensitivity is not lost.

After the mapping, the density filter in Eq. (2) is applied to each volume fraction.

$$\tilde{v}_{ie} = \frac{\sum_{j\in\mathcal{N}_e} w_{ej} V_j v_{ij}}{\sum_{j\in\mathcal{N}_e} w_{ej} V_j}. \tag{22}$$

Because the density filter is an average with nonnegative weights, the relations in Eq. (21) are preserved after filtering. In particular, at a material-filled interface, the sum of the filtered volume fractions is unity, as in Eq. (12).

4.2 Projection applied separately to solid amount and composition

From the filtered volume fractions $\tilde{v}_i$ in Eq. (22), the solid amount s and the composition φ_i are obtained as follows:

$$\begin{cases} s = \sum_{i=1}^{n} \tilde{v}_i \\ \varphi_i = \dfrac{\tilde{v}_i}{s}. \end{cases} \tag{23}$$

The solid amount s represents the total amount of materials in the element, and the composition φ_i represents the fraction of the solid amount occupied by material i. Projection using the function in Eq. (5) is applied to these quantities separately, and the projected volume fraction $\bar{v}_i$ is obtained as follows:

$$\begin{cases} \bar{s} = H(s), \\ \psi_i = \dfrac{H_\varphi(\varphi_i)}{\sum_{k=1}^{n} H_\varphi(\varphi_k)}, \\ \bar{v}_i = \bar{s}\,\psi_i, \end{cases} \tag{24}$$

where $\bar{s}$ and ψ_i are the projected solid amount and the projected composition, respectively. H and H_φ are the functions of Eq. (5) used for the solid amount and the composition, respectively; they have the same threshold, and their projection sharpness parameters may take different values. $\varphi_i = 1/n$ is used at $s = 0$ because the composition is undefined in this case. According to Eq. (24), the sum of the projected volume fractions satisfies the following relation regardless of the number of materials:

$$\sum_{i=1}^{n} \bar{v}_i = \bar{s} \leq 1. \tag{25}$$

In material-filled states, $s = 1$, Eq. (5) gives $\bar{s} = H(1) = 1$, so the solid amount is preserved, and only the composition approaches 0 or 1. In addition, for a single material, Eq. (24) reduces to $\bar{v}_i = H(\tilde{v}_i)$ and coincides with ordinary projection.

If the projection is applied to each volume fraction separately, as in Eq. (4), whether a location is solid or void will be determined for each material. Therefore, the result changes depending on how the materials are divided in their definition, even for the same solid amount. If the projection is applied to the solid amount as in Eq. (24), this judgment will not depend on how the materials are divided. The difference between the two is shown numerically in Section 7.3. Researchers have proposed methods in which each phase has its own design variable field and is projected independently; these approaches include multiple-phase projection[32] for two phases

(solid and void) and its extension to multiple materials[31]. However, these methods aim to control the minimum length scale of each phase; they do not apply the projection separately to the solid amount and the composition.

4.3 Mixture rule

Given the projected solid amount $\bar{s}$ and the projected composition ψ_i in Eq. (24), Young's modulus is expressed as follows:

$$\begin{cases} E = \left(1 - \bar{s}^{\,p}\right) E_0 + \bar{s}^{\,p}\, M_q \\ M_q = \left(\sum_{i=1}^{n} \psi_i E_i^{\,q}\right)^{1/q}, \end{cases} \tag{26}$$

where M_q is Young's modulus for the solid part and is the power mean of Young's moduli for the materials weighted by the composition. p is the penalty exponent for the intermediate densities between solid and void, and $q\,(\neq 0)$ is the penalty exponent for material mixing; the two are given separately. For a single material, Eq. (26) coincides with SIMP.

From the properties of the power mean, M_q (Eq. (26)) satisfies the following relation for all q:

$$\min_i E_i \leq M_q \leq \max_i E_i. \tag{27}$$

At a material-filled interface ($\bar{s} = 1$), Eq. (26) gives Young's modulus as $E = M_q$. Therefore, according to Eq. (27), Young's modulus at the interface does not fall below that in the less stiff material. In addition, the following relation holds for $q < 1$, where equality holds only in single-material states:

$$M_q \leq \sum_{i=1}^{n} \psi_i E_i. \tag{28}$$

The right-hand side is the Young's modulus value given by the linear mixture rule. Thus, material mixing is penalized for $q < 1$ regardless of the combination of material property values (Eq. (28)). Because M_q is nondecreasing with respect to q, the penalty strengthens as q decreases. $q = 1$ and $q = -1$ coincide with the Voigt mixture rule (linear mixture rule) and the Reuss mixture rule (harmonic mean), respectively[9], and $q < -1$ gives a stronger penalty than the Reuss rule. Figure 2 shows Young's modulus at a material-filled interface in comparison with that under DMO (Eq. (15)).

In the optimization problem (6), SCMI uses $m_i = \bar{v}_i$ as the material i amount and calculates Young's modulus via Eq. (26). Because the same $\bar{\boldsymbol{v}}$ in Eq. (24) is used for both the stiffness and volume constraints, the evaluation discrepancy between the stiffness and volume described in Section 3 does not arise.

4.4 Symmetry of material definition

A permutation of the material numbers is denoted by π. Each step in SCMI behaves as follows under a permutation of the material numbers: The mapping satisfies the

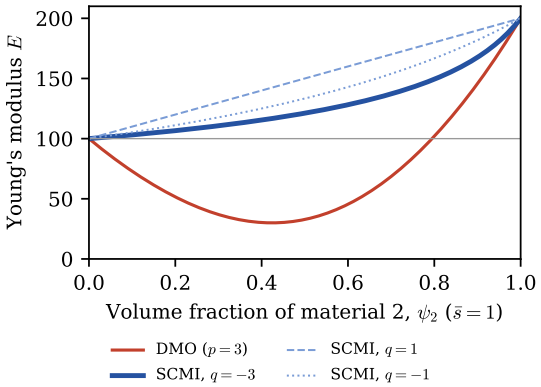


Fig. 2: Relation between volume fraction of material 2 and Young's modulus at interface filled with material 1 ($E_1 = 100$) and material 2 ($E_2 = 200$). The Eq. (15) result of DMO ($p = 3$, $t = \psi_2$) and Eq. (26) result of SCMI ($q = 1, -1, -3$) are shown.

following equation, and the density filter acts on the volume fractions of all materials in the same manner:

$$\mathcal{M}(\pi \boldsymbol{x}) = \pi \mathcal{M}(\boldsymbol{x}). \tag{29}$$

In the projection of Eq. (24), the solid amount is a sum and hence does not change, and the composition is permuted in the same manner. As the power mean of the mixture rule (26) is also a sum, it likewise does not change.

$$\sum_{i=1}^{n} \psi_{\pi(i)} \, E_{\pi(i)}^{q} = \sum_{i=1}^{n} \psi_i \, E_i^q. \tag{30}$$

Therefore, the optimization problem where the material definitions are permuted together with their property values and the upper limits of the volume constraints is the same as the original problem with permuted design variables. When the optimization algorithm iterations consist of operations that are invariant under the permutation of the design variables and constraint functions, the design variables at every iteration are also permuted in the same manner under exact arithmetic, and hence the same optimal structure is obtained. In other words, SCMI maintains the symmetry of material definition, as does DMO. By contrast, extended SIMP does not have this property (Appendix A).

5 Sensitivity analysis

Gradient-based optimization algorithms require the sensitivities of the objective and constraint functions to the design variables. In this section, the sensitivity of the SCMI objective function is derived through the adjoint variable method.

Under SCMI, the projected volume fractions $\bar{\boldsymbol{v}}$ are obtained from the design variables $\boldsymbol{x}$ through the mapping (19), density filter (22), and projection (24) (Eq. (16)), and $\bar{\boldsymbol{v}}$ affects the global stiffness matrix and displacement through Young's modulus

(Eq. (26)). $\bar{\boldsymbol{V}}$ is a vector consisting of the $\bar{v}_i$ of all elements; likewise, $\tilde{\boldsymbol{V}}$, $\boldsymbol{V}$, and $\boldsymbol{X}$ are vectors consisting of $\tilde{\boldsymbol{v}}$, $\boldsymbol{v}$, and $\boldsymbol{x}$, respectively. With the objective function written as $f(\bar{\boldsymbol{V}}, \boldsymbol{U})$, its sensitivity to the design variables is expressed by the chain rule as follows:

$$\frac{\partial f}{\partial \boldsymbol{X}} = \left(\frac{\partial \boldsymbol{V}}{\partial \boldsymbol{X}}\right)^{\mathrm{T}} \left(\frac{\partial \tilde{\boldsymbol{V}}}{\partial \boldsymbol{V}}\right)^{\mathrm{T}} \left(\frac{\partial \bar{\boldsymbol{V}}}{\partial \tilde{\boldsymbol{V}}}\right)^{\mathrm{T}} \frac{\mathrm{d}f}{\mathrm{d}\bar{\boldsymbol{V}}}, \tag{31}$$

where $\mathrm{d}f/\mathrm{d}\bar{\boldsymbol{V}}$ is the total derivative, including the dependence of displacement $\boldsymbol{U}$ on $\bar{\boldsymbol{V}}$. In the following, the terms on the right-hand side of Eq. (31) are derived in sequence from the right side.

First, $\mathrm{d}f/\mathrm{d}\bar{\boldsymbol{V}}$ is obtained via the adjoint variable method. For the objective function $f(\bar{\boldsymbol{V}}, \boldsymbol{U})$, the Lagrangian L is defined by introducing the adjoint variable $\boldsymbol{\lambda}$ and the equilibrium equation in Eq. (6).

$$L(\bar{\boldsymbol{V}}, \boldsymbol{U}, \boldsymbol{\lambda}) = f(\bar{\boldsymbol{V}}, \boldsymbol{U}) + \boldsymbol{\lambda}^{\mathrm{T}}\big(\boldsymbol{K}\boldsymbol{U} - \boldsymbol{F}_{\mathrm{ext}}\big). \tag{32}$$

Because L is equivalent to f when the equilibrium equation is satisfied, $\mathrm{d}f/\mathrm{d}\bar{\boldsymbol{V}} = \mathrm{d}L/\mathrm{d}\bar{\boldsymbol{V}}$ holds. Assuming that the external force vector $\boldsymbol{F}_{\mathrm{ext}}$ does not depend on the design variables, the total derivative of L is given as follows:

$$\frac{\mathrm{d}L}{\mathrm{d}\bar{\boldsymbol{V}}} = \left(\frac{\partial f}{\partial \bar{\boldsymbol{V}}}\right)_{\mathrm{ex}} + \boldsymbol{\lambda}^{\mathrm{T}} \frac{\partial \boldsymbol{K}}{\partial \bar{\boldsymbol{V}}} \boldsymbol{U} + \left(\frac{\partial f}{\partial \boldsymbol{U}} + \boldsymbol{\lambda}^{\mathrm{T}} \boldsymbol{K}\right) \frac{\partial \boldsymbol{U}}{\partial \bar{\boldsymbol{V}}}, \tag{33}$$

where $(\cdot)_{\mathrm{ex}}$ denotes the explicit derivative term. $\partial \boldsymbol{U}/\partial \bar{\boldsymbol{V}}$ is an implicit derivative term, and its direct computation requires solving as many systems of linear equations as there are design variables. Therefore, the following adjoint equation is applied so that the coefficient of this term becomes $\boldsymbol{0}$:

$$\boldsymbol{K}^{\mathrm{T}} \boldsymbol{\lambda} = -\left(\frac{\partial f}{\partial \boldsymbol{U}}\right)^{\mathrm{T}}. \tag{34}$$

Given the adjoint variable satisfying Eq. (34), the sensitivity of the objective function is obtained using the following equation, which contains no implicit derivative term:

$$\frac{\mathrm{d}f}{\mathrm{d}\bar{\boldsymbol{V}}} = \left(\frac{\partial f}{\partial \bar{\boldsymbol{V}}}\right)_{\mathrm{ex}} + \boldsymbol{\lambda}^{\mathrm{T}} \frac{\partial \boldsymbol{K}}{\partial \bar{\boldsymbol{V}}} \boldsymbol{U}. \tag{35}$$

The objective function in Eq. (6) does not depend explicitly on $\bar{\boldsymbol{V}}$, and $\partial f/\partial \boldsymbol{U} = \boldsymbol{F}_{\mathrm{ext}}^{\mathrm{T}}/f_0$. Because the global stiffness matrix is symmetric, the solution of Eq. (34) is $\boldsymbol{\lambda} = -\boldsymbol{U}/f_0$, and the adjoint equation need not be solved separately. Therefore, from Eq. (35), the sensitivity of the objective function to the volume fraction $\bar{v}_{ie}$ of material i in element e is as follows:

$$\frac{\mathrm{d}f}{\mathrm{d}\bar{v}_{ie}} = -\frac{1}{f_0} \boldsymbol{U}^{\mathrm{T}} \frac{\partial \boldsymbol{K}}{\partial \bar{v}_{ie}} \boldsymbol{U}. \tag{36}$$

Because the Poisson's ratio is constant in this study, the elasticity matrix in Eq. (7) can be written as $\boldsymbol{C}(E) = E\,\boldsymbol{C}_0$, where $\boldsymbol{C}_0$ is the elasticity matrix for a unit Young's modulus. Therefore, the derivative of the global stiffness matrix is as follows:

$$\frac{\partial \boldsymbol{K}}{\partial \bar{v}_{ie}} = \frac{\partial E}{\partial \bar{v}_i} \int_{\Omega_e} \boldsymbol{B}^{\mathrm{T}} \boldsymbol{C}_0 \boldsymbol{B}\, \mathrm{d}\Omega. \tag{37}$$

The derivative $\partial E/\partial \bar{v}_i$ of Young's modulus in element e is obtained by substituting $\bar{s} = \sum_{k=1}^{n} \bar{v}_k$ and $\psi_k = \bar{v}_k/\bar{s}$ into Eq. (26) and differentiating, which gives the following equation:

$$\frac{\partial E}{\partial \bar{v}_i} = p\,\bar{s}^{\,p-1}\big(M_q - E_0\big) + \frac{\bar{s}^{\,p-1}}{q}\, M_q^{1-q}\big(E_i^q - M_q^q\big). \tag{38}$$

The first term on the right-hand side has the same form as in SIMP and corresponds to a change in the solid amount, and the second term corresponds to a change in the composition.

Next, the derivative term for the projection (24) is obtained. With the sensitivity of Eq. (36) in element e written as $\gamma_i = \mathrm{d}f/\mathrm{d}\bar{v}_{ie}$, sensitivity to the filtered volume fraction $\tilde{v}_{je}$ is given by the following equations:

$$\begin{cases} \dfrac{\partial f}{\partial \tilde{v}_{je}} = H'(s)\,\alpha + \dfrac{\bar{s}}{s}\Big(b_j - \displaystyle\sum_{k=1}^{n} b_k\,\varphi_k\Big) \\[2ex] \alpha = \displaystyle\sum_{i=1}^{n} \gamma_i\,\psi_i \\[2ex] b_k = \dfrac{H'_\varphi(\varphi_k)\,(\gamma_k - \alpha)}{\sum_{m=1}^{n} H_\varphi(\varphi_m)}, \end{cases} \tag{39}$$

The first (second) term on the right-hand side of the first equation corresponds to a change in the solid amount (composition). H' and H'_φ are the derivatives of the function of Eq. (5) and are given as follows:

$$H'(a) = \frac{\beta\,\big(\mathrm{sech}(\beta(a-\eta))\big)^2}{\tanh(\beta\eta) + \tanh(\beta(1-\eta))}. \tag{40}$$

Subsequently, the derivative term for the density filter (22) is obtained. The density filter is linear in the volume fractions and is expressed by the following equations:

$$\begin{cases} \tilde{\boldsymbol{V}}_i = \boldsymbol{W}\boldsymbol{V}_i \\[2ex] W_{ej} = \begin{cases} \dfrac{w_{ej}\,V_j}{\sum_{k\in\mathcal{N}_e} w_{ek}\,V_k} & (j \in \mathcal{N}_e) \\[2ex] 0 & (j \notin \mathcal{N}_e), \end{cases} \end{cases} \tag{41}$$

where $\boldsymbol{V}_i$ and $\tilde{\boldsymbol{V}}_i$ are vectors consisting of the elementwise values of the material i volume fraction, and $\boldsymbol{W}$ is a matrix of the weights of the density filter. Because $\boldsymbol{W}$

does not depend on the design variables, the derivative term for the density filter is as follows:

$$\frac{\partial f}{\partial \boldsymbol{V}_i} = \boldsymbol{W}^{\mathrm{T}} \frac{\partial f}{\partial \tilde{\boldsymbol{V}}_i}. \tag{42}$$

Finally, the derivative term for the mapping (19) is obtained. Given $D = \omega_0 + \sum_{k=1}^{n} \omega_k$ in element e, the derivatives of the volume fractions with respect to the design variables are given by the following equations:

$$\frac{\partial v_i}{\partial x_k} = \frac{1}{D}\Big(\frac{\partial \omega_i}{\partial x_k} - v_i \frac{\partial D}{\partial x_k}\Big), \tag{43}$$

$$\frac{\partial \omega_i}{\partial x_k} = \begin{cases} \displaystyle\prod_{\substack{j=1 \\ j\neq i}}^{n} (1 - x_j) & (k = i) \\ \displaystyle -x_i \prod_{\substack{j=1 \\ j\neq i,\, k}}^{n} (1 - x_j) & (k \neq i), \end{cases} \tag{44}$$

$$\frac{\partial \omega_0}{\partial x_k} = -\prod_{\substack{j=1 \\ j\neq k}}^{n} (1 - x_j), \tag{45}$$

$$\frac{\partial D}{\partial x_k} = \frac{\partial \omega_0}{\partial x_k} + \sum_{i=1}^{n} \frac{\partial \omega_i}{\partial x_k}. \tag{46}$$

Therefore, from Eqs. (42) and (43), the sensitivity of the objective function to the design variables is obtained as follows:

$$\frac{\partial f}{\partial x_{ke}} = \sum_{i=1}^{n} \frac{\partial f}{\partial v_{ie}} \frac{\partial v_i}{\partial x_k}. \tag{47}$$

6 Verification of sensitivity analysis

In gradient-based topology optimization, the optimal structure is derived on the basis of the sensitivities of the evaluation functions to the design variables, so accurate sensitivities must be used in the computation. Here, the sensitivity formulated in the previous section is validated by comparing it with the sensitivity distribution obtained via the finite difference method. The latter sensitivity is obtained as the central difference of the evaluation function by the following equation:

$$\frac{\partial f}{\partial x_{ie}} = \frac{f(\boldsymbol{X} + \Delta x\, \hat{\boldsymbol{e}}_{ie}) - f(\boldsymbol{X} - \Delta x\, \hat{\boldsymbol{e}}_{ie})}{2\Delta x}. \tag{48}$$

Δx is a small perturbation of the design variable, and $\hat{\boldsymbol{e}}_{ie}$ is a vector whose component for material i in element e is 1 and whose other components are all 0. The finite difference method evaluates the function twice for each design variable, so it

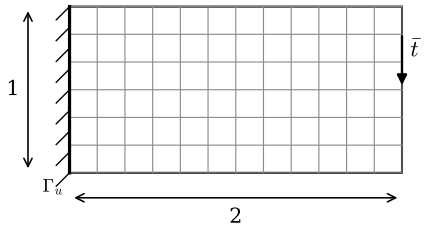


Fig. 3: Analysis model used for verification of sensitivity analysis.

increases in computational cost and becomes impractical as the number of design variables increases. However, it is used as the verification benchmark because it computes sensitivity with high accuracy regardless of the evaluation function.

6.1 Analysis model and conditions

The two-dimensional 2×1 rectangular model in Fig. 3 is used for verification. The model used for finite element analysis consists of $12 \times 6 = 72$ four-node bilinear quadrilateral elements. The boundary condition is set to the cantilever condition; the left end is fully fixed, a downward concentrated load of magnitude 1.0 is applied to the node at the center of the right end, and the material model is an isotropic linear elastic body in the two-dimensional plane stress state. The material properties are listed in Table 1. A multimaterial problem with two materials is considered, and the number of design variables is 144, which is twice the number of elements, 72. Assuming a more general condition, the initial design variable distribution is given by uniform random numbers in the range $[0.1, 0.9]$ for each element and material. The filter radius is set to $R = 4h$ using the element side length h, the projection sharpness parameter to $\beta = 5$, the threshold to $\eta = 0.5$, the penalty exponent to $p = 3$, and the penalty exponent for material mixing to $q = -3$. The perturbation of the design variable in the finite difference method is set to $\Delta x = 1.0 \times 10^{-6}$.

6.2 Verification results

Figure 4 compares the sensitivity of the objective function formulated in Section 5 with the sensitivity distribution obtained by the finite difference method. Figures 4(a) and (b) show the sensitivities of the objective function to the design variables of materials 1 and 2, respectively. The sensitivity distributions obtained by the two methods agree across all design variables, confirming that the formulated sensitivity is obtained with high accuracy. The relative L_2 error of sensitivity over all design variables is 2.06×10^{-7}, and sensitivity is computed accurately. Hence, the sensitivity formulated in this paper is accurate and can be used in the subsequent topology optimization.

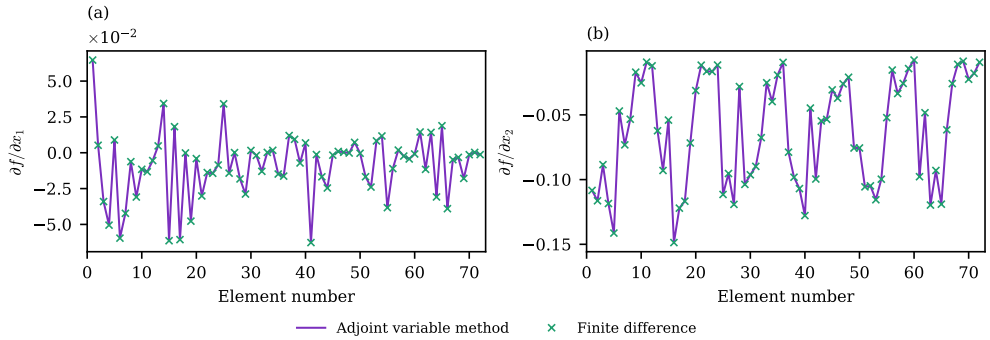


Fig. 4: Comparison of sensitivity distributions of objective function obtained via adjoint variable and finite difference methods. Sensitivity to (a) x_1 and (b) x_2.

7 Numerical example 1: evaluation of stiffness at material interface

In this section, binarized design variables are given without optimization, and Young's modulus at the interface is evaluated through interpolation via each scheme. This confirms the occurrence of stiffness reduction under DMO (Section 3) and its absence under SCMI. In addition, the effect of applying the projection separately to the solid amount and the composition under SCMI is confirmed.

7.1 Analysis model and conditions

A two-dimensional 200×100 rectangular model is used for this analysis. The left half of the domain is material 1, the right half is material 2, and the design variables are set to $(x_1, x_2) = (1, 0)$ in the left half and $(x_1, x_2) = (0, 1)$ in the right half. This is the state of the binarized design variables assumed in Section 3. The material boundary coincides with the element edges.

The analysis model is discretized using four-node bilinear quadrilateral elements, and a mesh of 20×10 elements is used so that the distribution of Young's moduli at interfaces can be shown relative to element size. An isotropic linear elastic body in the plane stress state is assumed, and the material properties are listed in Table 1. The Young's modulus value of void is set to $E_0 = 1.0 \times 10^{-3}$, and the penalty exponent is $p = 3$. The filter radius is set to $R = 2h, 4h$ using the element side length h, the projection sharpness parameter to $\beta = 1, 5, 32$, and the threshold to $\eta = 0.5$.

Young's modulus is obtained from these design variables using the procedure of each scheme. For DMO, the density filter of Eq. (2), the projection of Eq. (4), and the material interpolation of Eq. (8) are applied in this order. For SCMI, the mapping of Eq. (19), the density filter of Eq. (22), the projection of Eq. (24), and the material interpolation of Eq. (26) are adopted in this sequence. Young's modulus is evaluated in the element row at mid-height, as indicated by the dashed-line frame in Fig. 5(b). The penalty exponent for material mixing under SCMI is set to $q = -3$.

Table 1: Material properties.

	Young's modulus	Poisson's ratio
Material 1	100	0.3
Material 2	200	0.3

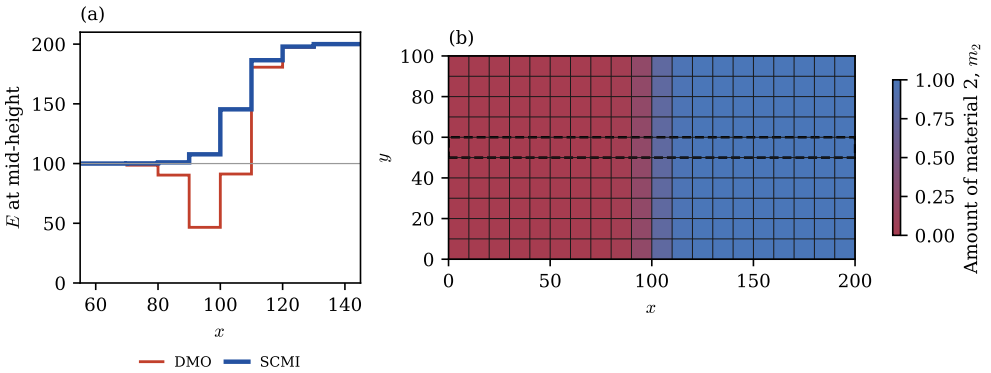


Fig. 5: Interface at straight material boundary ($R = 4h$, $\beta = 5$). (a) Young's modulus in element row at mid-height crossing interface. (b) Finite element mesh of whole analysis model and amount m_2 of material 2 (the dashed-line frame indicates the element row where Young's modulus is evaluated). The m_2 distribution is identical between DMO and SCMI.

7.2 Young's modulus at interface

Figure 5(a) shows the Young's modulus distribution under each scheme at $R = 4h$ and $\beta = 5$, and Fig. 5(b) shows the finite element mesh of the whole analysis model and the distribution of the amount of material 2. Under DMO, Young's modulus decreases at the interface and becomes lower than that of the material on either side of the interface (Fig. 5(a)). This is the stiffness reduction shown by Eq. (15). By contrast, under SCMI, Young's modulus at the interface lies between the moduli of the materials on both sides and is equal to or greater than that of material 1, which is less stiff. This is because the solid amount at the interface remains unity (Eq. (25)) and the power mean value is between E_1 and E_2 (Eq. (27)).

Figure 6 shows the Young's modulus distribution under DMO per filter radius R and projection sharpness parameter β. Young's modulus at the interface is lower at a larger R and a smaller β. In other words, Young's modulus at the interface under DMO is determined not by material properties but by the filter radius and the projection sharpness parameter. By contrast, Young's modulus at the interface under SCMI is equal to or greater than that of material 1 under all conditions.

The above results confirm that DMO evaluates the structure on the premise that stiffness decreases at the interface and the designer cannot specify the reduction amount, whereas this stiffness reduction does not occur under SCMI.

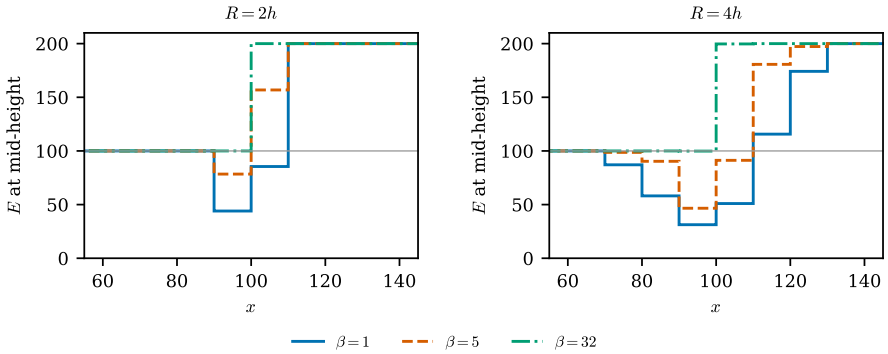


Fig. 6: Young's modulus under DMO in element row at mid-height crossing straight material boundary for different filter radii R and projection sharpness parameters β.

Table 2: Solid amount after projection for filtered volume fractions $\tilde{\boldsymbol{v}}$. Per volume fraction: $\bar{v}_i = H(\tilde{v}_i)$. SCMI: Eq. (24). $\beta = 5$, $\eta = 0.5$.

State	Filtered volume fractions $\tilde{\boldsymbol{v}}$	Solid amount after projection	
		Per volume fraction $\sum_i H(\tilde{v}_i)$	SCMI $H\left(\sum_i \tilde{v}_i\right)$
Mixture with 60% solid	$(0.3, 0.3)$	2.28×10^{-1}	7.34×10^{-1}
Initial design $\boldsymbol{x} = (1/2, 1/2)$	$(1/3, 1/3)$	3.08×10^{-1}	8.46×10^{-1}
Filled three-material mixture	$(1/3, 1/3, 1/3)$	4.63×10^{-1}	1.00

7.3 Effect of variables to which Heaviside projection is applied

Under SCMI, the projection is applied separately to the solid amount s and the composition φ_i (Eq. (24)). The effect of this process on optimization is verified by comparing its result with that of applying the projection to each volume fraction (Eq. (4)) ($\bar{v}_i = H(\tilde{v}_i)$). The projected solid amount $\sum_{i=1}^{n} \bar{v}_i$ is computed for the filtered volume fractions $\tilde{\boldsymbol{v}}$ of three representative states. The projection sharpness parameter is set to $\beta = 5$ and the threshold to $\eta = 0.5$. The results are listed in Table 2.

When the projection is applied to each volume fraction, the solid amount is evaluated as smaller than that under SCMI in every state (Table 2). For the mixture with 60% solid, the SCMI value coincides with $H(0.6)$, which is the value obtained when the same 60% solid is regarded as a single material. When the projection is applied to each volume fraction, the solid amount is evaluated as smaller, merely because the same amount of solid is divided into two materials. For the mixture filled with the three materials, SCMI keeps the solid amount at unity, whereas it is evaluated as less than half this value when the projection is applied to each volume fraction. In addition, the initial design variables $\boldsymbol{x} = (1/2, 1/2)$ are mapped to $\tilde{\boldsymbol{v}} = (1/3, 1/3)$ via Eq. (19). Moreover, in this state, the solid amount is evaluated as smaller when the projection is applied to each volume fraction, so the optimization starts from a state

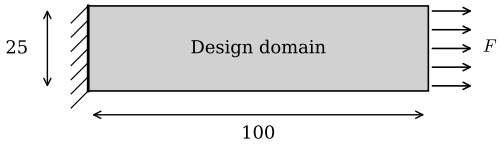


Fig. 7: Fixed design domain and boundary conditions of tensile bar.

with a small solid amount. In the two-material state, the two approaches coincide because $H(a) + H(1-a) = 1$ holds for $\eta = 0.5$.

These results verify that applying the projection to the solid amount makes the solid/void judgment independent of how the materials are divided in definition and of the material number.

8 Numerical example 2: tensile bar

8.1 Analysis model and conditions

Optimization results for a tensile bar show that SCMI does not reduce stiffness at the interface and yields an optimal structure similar to that of extended SIMP. This section clarifies the differences in the results of DMO, SCMI ($q = -3$), and extended SIMP. Young's modulus under extended SIMP is calculated using Eq. (A4). A tensile bar of length 100 and height 25 (Fig. 7) is considered as a fixed design domain. The left end is fully fixed, and a uniformly distributed load in the x direction with a total magnitude of 1.0 is applied to the entire right end. A mesh of 160×40 elements is used. The element type, material properties, Young's modulus of void, and penalty exponent are the same as in numerical example 1. The filter radius is $R = 4h$, the projection sharpness parameter is $\beta = 5$, and the threshold is $\eta = 0.5$. The upper limits of the material volume constraints are set to $\bar{V}_1 = \bar{V}_2 = 0.25$. The amount m_i of material i under each scheme is $m_i = \bar{x}_i$ for DMO, $m_i = \bar{v}_i$ for SCMI, and Eqs. (A2) and (A3) for extended SIMP. The volume constraints are imposed on the integral of m_i under all schemes. The materials are defined in ascending order of stiffness. This is the order in which material mixing is penalized under extended SIMP.

The initial design variable distribution is uniformly 0.5 throughout the fixed design domain under all schemes. This is because, when the initial design variables differ greatly from the projection threshold $\eta = 0.5$, the derivative of the Heaviside function becomes small, which makes the sensitivities with respect to all design variables small and stalls the optimization. The lower bound of the design variables is set to $x_{\min} = 1.0 \times 10^{-4}$ under all schemes. The upper bound is set to $x_{\max} = 1$ under DMO and extended SIMP, and $\varepsilon = 1.0 \times 10^{-4}$ is used in Eq. (20) under SCMI. Ipopt[33] is used as the optimization algorithm. The maximum number of optimization steps, which is the termination condition of the optimization, is set to 300.

8.2 Optimization results

The material and Young's modulus distributions of the optimal structures are shown in Table 3. In the material distributions, gray represents void, red represents material 1 (lower stiffness), and blue represents material 2 (higher stiffness). The material distribution N_{mat} is computed based on the interpolation of each scheme. Specifically, under DMO and extended SIMP, it is computed using Eqs. (8) and (A1), respectively, with the Young's moduli of void and material i being replaced by $E_0 = 0$ and $E_i = i$ and with the penalty exponent being $p = 1$. The following equation, obtained similarly from Eq. (26) at $p = q = 1$, is used under SCMI to indicate the presence of the materials at each location.

$$N_{\mathrm{mat}} = \sum_{i=1}^{n} i\,\bar{v}_i. \tag{49}$$

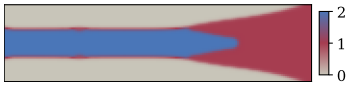
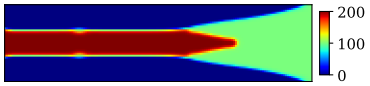
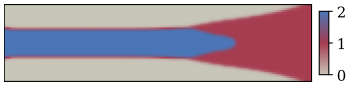
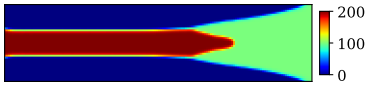
$\bar{v}_i$ is the projected volume fraction of Eq. (24). Under SCMI, this volume fraction indicates the presence of the material at that location. SCMI and extended SIMP yield similar, mechanically reasonable structures (Table 3). The whole structure is a single bar extending in the tensile direction and is divided into material 2 (higher stiffness) on the left (fixed) side and material 1 on the right (loaded) side. The compliance of the optimized structure is 5.95×10^{-2} under SCMI and 5.92×10^{-2} under extended SIMP, and the two are comparable, with a difference of 0.5 %. DMO results in a different structural layout. Material 1 is on the fixed-end side, and material 2 is beyond it; the two materials are arranged in series, and the loaded end is connected by thin members of both materials 1 and 2. Its compliance, 6.32×10^{-2}, is 6.2 % higher than that under the proposed SCMI. This difference includes the effect of the Young's modulus reduction at the interfaces in addition to the difference in structural layout. Furthermore, as shown by the Young's modulus distributions in Table 3, the modulus at the interfaces between the two materials is very low in the optimal structure of DMO—the drawback of this scheme manifesting in the optimization result. Under extended SIMP and the proposed SCMI, stiffness does not reduce at the interfaces between the materials, and the materials are properly connected. The above results suggest that the proposed SCMI avoids the artificial stiffness reduction at the interfaces between materials—a drawback of DMO—and yields a mechanically reasonable optimization result with a shape similar to and a compliance comparable to those of the widely used extended SIMP.

9 Numerical example 3: cantilever beam

9.1 Analysis model and conditions

The two-dimensional 200×100 rectangular model in Fig. 8 is adopted as a fixed design domain. The left end is fully fixed, and a downward distributed load of magnitude 0.4 is applied to a region of width 5.0 at the center of the right end. A mesh of 150×75 elements is used. The upper limits of the volume constraints are set to $\bar{V}_i = 0.2$ for both materials 1 and 2. The other conditions are the same as in numerical example 2. In the following, the optimization results with the basic parameters are presented first,

Table 3: Optimal structures of tensile bar.

Method	Material number	Young's modulus
DMO		
SCMI		
Extended SIMP		

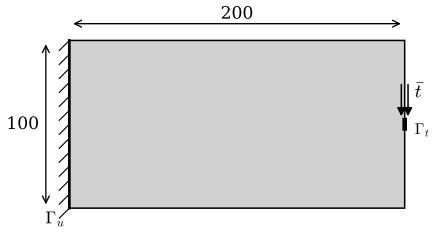


Fig. 8: Fixed design domain and boundary conditions of cantilever beam.

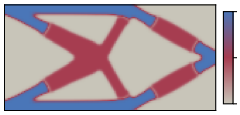
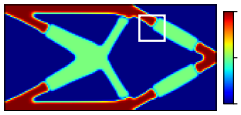
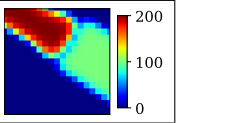
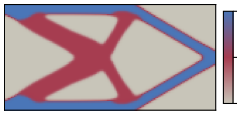
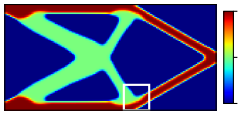
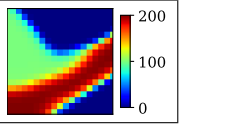
followed by examinations of the effect of the penalty exponent q for material mixing and the symmetry of material definition. Unless otherwise stated, the materials are defined in ascending order of stiffness (Table 1).

9.2 Optimization results

The material and Young's modulus distributions of the optimal structures obtained by DMO and SCMI with a $q = -3$ penalty exponent for material mixing are shown in Table 4. The white box and its enlarged view in Table 4 show part of the interface between materials 1 and 2. As in the case of the tensile bar, under DMO, Young's modulus decreases at every location where the members of materials 1 and 2 are joined, and the members are almost separated by low-stiffness regions. By contrast, this reduction in Young's modulus does not occur in the proposed SCMI, and the two materials are connected.

Note that joint stiffness may decrease in actual multimaterial structures. DMO may appear to represent this reduction; however, the magnitude of stiffness reduction under DMO depends on the filter radius and projection sharpness parameter and cannot be specified by the designer (Fig. 6). To account for the stiffness reduction at a joint, the designer should provide its characteristics explicitly, as in methods that specifically define interface properties[28–30]. Because such unintended stiffness

Table 4: Optimal structures of cantilever beam.

Method	Material number	Young's modulus	Enlarged view
DMO			
SCMI			

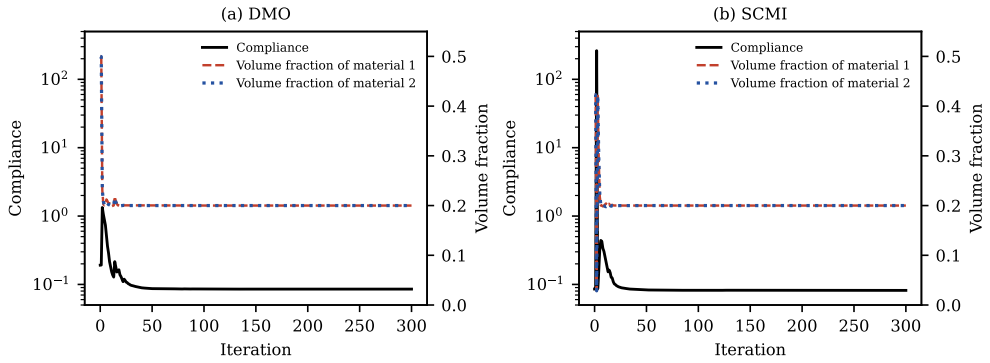


Fig. 9: Optimization histories of (a) DMO and (b) SCMI. The left axis is the compliance (evaluated through interpolation via each scheme), and the right axis is the volume fractions of materials 1 and 2.

reduction at joints does not occur under SCMI, it can be used as a basis for such methods.

Figure 9 shows the histories of the compliance and volume fractions of materials 1 and 2 under DMO and SCMI optimization. The objective function changes little over the last 100 steps, converging to an almost constant value under both DMO and SCMI. Thus, the number of optimization steps required for convergence is comparable to that under DMO, and no major problem occurs.

9.3 Examination of material separation

The effect of the penalty exponent q for material mixing under SCMI on material separation is examined. The binarization and separation of each material are evaluated using the grayscale measure[34] of the amount m_i of material i.

$$G_i = \frac{1}{N_{\mathrm{elem}}} \sum_{e=1}^{N_{\mathrm{elem}}} 4\, m_{ie}\,(1 - m_{ie}). \tag{50}$$

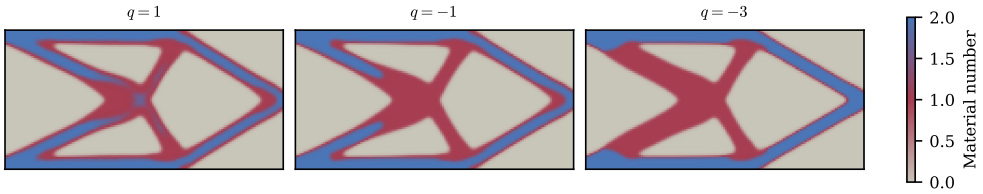


Fig. 10: Material number of optimal structures of cantilever beam obtained by SCMI with different penalty exponents q for material mixing (values interpolated linearly with 0 for void, 1 for material 1, and 2 for material 2).

Table 5: Grayscale measure of optimal structures of cantilever beam obtained by SCMI with different penalty exponents q for material mixing and by DMO.

	SCMI ($q = 1$)	SCMI ($q = -1$)	SCMI ($q = -3$)	DMO
G_1	2.32×10^{-1}	1.82×10^{-1}	6.62×10^{-2}	7.56×10^{-2}
G_2	1.39×10^{-1}	1.03×10^{-1}	6.91×10^{-2}	6.67×10^{-2}

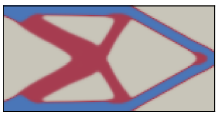
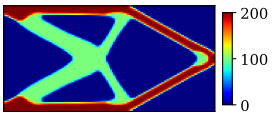
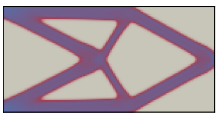
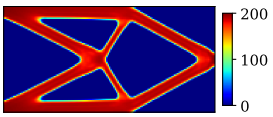
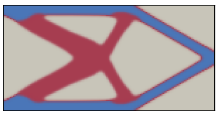
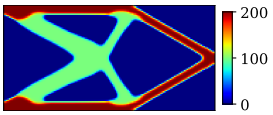
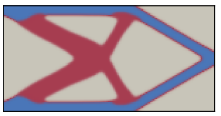
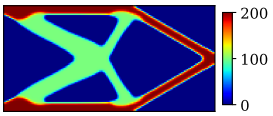
G_i is 0 when m_i is 0 or 1 in all elements and increases when the solid–void boundary is unclear or when the two materials mix. Note that G_i does not become 0; because of the filtering, elements in which m_i takes intermediate values always appear at the member contours and the material boundaries.

The material distributions of the optimal structures for $q = 1, -1, -3$ are shown in Fig. 10. The evaluation results of the grayscale measure of Eq. (50) are listed in Table 5 together with the result of DMO in Table 4. In the optimal structure for $q = 1$, material 1 (red) and material 2 (blue) are not separated (Fig. 10). At $q = -1$, material binarization progresses and the grayscale measure decreases with q; for $q = -3$, the grayscale measure decreases greatly relative to that at $q = -1$. This is comparable to the value under DMO. Additionally, under SCMI with $q = -3$, each material is binarized and clearly separated to the same degree as under DMO. These results suggest that the material mixing penalty $q = -1$ is insufficient, and a smaller value must be given. Hence, $q = -3$ is used as the basic parameter in this study.

9.4 Examination of symmetry of material definition

For SCMI ($q = -3$) and extended SIMP, optimization is performed under swapped definitions of materials 1 and 2 (material 1 with $E = 200$ and material 2 with $E = 100$). The other analysis conditions are the same as in the preceding sections. The results are shown in Table 6, where the order $(1, 2)$ denotes the original order of material definition and $(2, 1)$ denotes the swapped order. Regardless of the definition order, the material numbers are assigned such that the material with Young's modulus 100 is 1 and the material with Young's modulus 200 is 2. Under extended SIMP, the optimal structure changes greatly when the order of material definition is swapped (Table 6).

Table 6: Optimal structures of cantilever beam under swapped order of material definition.

Method	Order	Material number	Young's modulus
Extended SIMP	$(1, 2)$		
	$(2, 1)$		
SCMI	$(1, 2)$		
	$(2, 1)$		

In this case, $E_1 = 200$ and $E_2 = 100$ in Eq. (A4), and Young's modulus is given by the following equation:

$$E = E_0 + (200 - E_0)\,\bar{x}_1^{\,p} - 100\,\bar{x}_1^{\,p}\,\bar{x}_2^{\,p}. \tag{51}$$

This expression exceeds the linear mixture rule (A6) for intermediate $\bar{x}_2$ (Appendix A), so material mixing is advantageous. Consequently, the optimal structure becomes grayscale, with the two materials mixed throughout the structure, and a structure with binarized materials is not obtained. Therefore, under extended SIMP, the optimization result depends on the order of material definition, and an appropriate optimization result cannot be obtained for some definitions. By contrast, under SCMI, the material layout of the optimal structure is the same as that for the original definition, even when the material numbers are swapped (Table 6). This is because the optimization problem of SCMI does not depend on the order of material definition (Eqs. (29) and (30)). Thus, under SCMI, the designer does not need to consider such order.

9.5 Application to three materials

Because the formulation of SCMI does not depend on the number of materials, it can be applied directly to problems with three or more materials. This advantage is confirmed by optimizing a cantilever beam with three materials.

The material properties are listed in Table 7. Materials 1 and 2 are the same as in the preceding sections, but material 3, with lower Young's modulus, is added. The upper limits of the volume constraints are set to $\bar{V}_i = 0.15$ for all materials. The other analysis conditions are the same as in the preceding sections. DMO and SCMI are used, and the penalty exponent for material mixing under SCMI is set to $q = -3$.

Table 7: Material properties used for cantilever beam with three materials.

	Young's modulus	Poisson's ratio
Material 1	100	0.3
Material 2	200	0.3
Material 3	50	0.3

Under SCMI, the symmetry of material definition is confirmed by performing three computations, with the order of material definition set to $(1, 2, 3)$, $(2, 3, 1)$, and $(3, 1, 2)$.

The material and Young's modulus distributions of the optimal structures are shown in Table 8. The material distributions are obtained in the same manner as in numerical example 2; gray represents void, red represents material 1, blue represents material 2, and yellow represents material 3. Regardless of the order of material definition, the material numbers are those in Table 7. The white box and its enlarged view in Table 8 show part of the interface between different materials. Under DMO, Young's modulus decreases at the interfaces between different materials, as in the case of two materials (Table 8). In particular, where the three materials meet, Young's modulus falls far below that of material 3, which has the lowest stiffness. This is because, as the second term on the right-hand side of Eq. (11) shows, the weight of void increases with the number of combinations of overlapping materials. By contrast, under SCMI, Young's modulus does not decrease at the interfaces in the three-material case either, and the materials are clearly separated in the obtained structure. In addition, the material layout of the optimal structure is the same under the three computations with different orders of material definition.

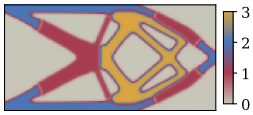
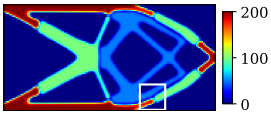
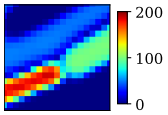
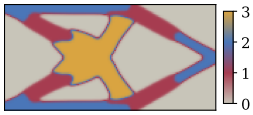
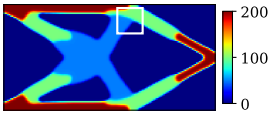
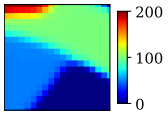
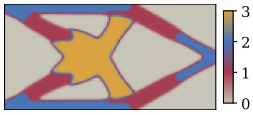
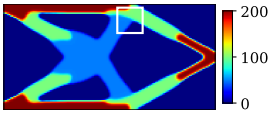
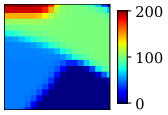
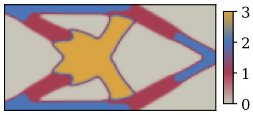
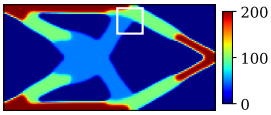
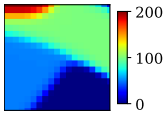
The above results suggest that, even in the three-material problem, SCMI yields an optimal structure that does not depend on the order of material definition, without stiffness reduction at the interfaces.

10 Conclusions

In this study, SCMI is proposed as a material interpolation scheme for multimaterial topology optimization. It maps design variables to volume fractions before filtering, separates the filtered volume fractions into the solid amount and the composition, and interpolates material properties using a Heaviside projection and a power-mean-based mixture rule. The resulting optimization does not depend on the order of material definition, and the stiffness at the interfaces between different materials is not artificially reduced by numerical parameters, such as the penalty exponent and filter radius. The findings of this study are as follows:

- The presented formulation combines (1) a mapping of the design variables to volume fractions before filtering with (2) a material interpolation separated into the solid amount and the composition. This formulation simultaneously maintains the symmetry of material definition, keeps Young's modulus at a material-filled interface between the moduli of the materials on both sides, and keeps the sum of the

Table 8: Optimal structures of cantilever beam with three materials.

Method	Order	Material number	Young's modulus	Enlarged view
DMO	$(1, 2, 3)$			
SCMI	$(1, 2, 3)$			
	$(2, 3, 1)$			
	$(3, 1, 2)$			

volume fractions of the materials at the same location at or below unity. The novelty of this study is that these properties are achieved without imposing additional constraints.

- The sensitivity of the SCMI objective function to design variables is formulated using the adjoint variable method and compared with the sensitivity obtained using the finite difference method. The alignment in their results shows that the proposed scheme gives correct sensitivities.
- The stiffness at interfaces is evaluated for a straight material boundary. Under SCMI, Young's modulus at a material-filled interface remains between the moduli of the materials on both sides, and no artificial stiffness reduction occurs at the interface.
- In the optimization of a tensile bar and a cantilever beam, no stiffness reduction occurs at the interfaces in the optimal structures obtained by SCMI. For the tensile bar, a mechanically reasonable optimal structure similar to that of the widely used extended SIMP is obtained. In addition, each material is binarized to the same degree as in DMO when the penalty exponent q for material mixing is sufficiently small.
- When the order of material definition is swapped, a structure with binarized materials is not obtained by extended SIMP, but the same optimal structure is obtained by SCMI. With SCMI, the designer does not need to consider the order of material definition.
- The optimization of a cantilever beam with three materials shows that SCMI is also applicable to three-material problems. In this case, no stiffness reduction occurs at interfaces, and the same optimal structure is obtained regardless of the order of material definition.

Declarations

Funding

The authors did not receive support from any organization for the submitted work.

Author contributions

Shun Ogawa contributed to the study conception and design, developed the method, implemented the code, and performed the numerical computations. The first draft of the manuscript was written by Shun Ogawa, and Katsuyuki Suzuki reviewed and commented on previous versions of the manuscript. All authors read and approved the final manuscript.

Conflict of interest

On behalf of all authors, the corresponding author states that there is no conflict of interest.

Ethics approval and Consent to participate

Not applicable.

Data availability

Data will be made available on request.

Appendix A Extended SIMP

This section presents the formulation of extended SIMP[2, 3] and explains that this method does not have symmetry of material definition.

In extended SIMP, the first design variable represents the solid amount, and the second and subsequent design variables determine the assigned materials in a fixed order. When the materials are defined in the order $1, 2, \cdots, n$, Young's modulus E is given by the following equation:

$$E = E_0 + \sum_{i=1}^{n} (E_i - E_{i-1}) \prod_{j=1}^{i} d(\bar{x}_j). \tag{A1}$$

$d(a) = a^p$ is the same penalty function as in Eq. (9). The amount m_i of material i is given by the following equations:

$$m_i = \left(1 - \bar{x}_{i+1}\right) \prod_{j=1}^{i} \bar{x}_j \quad (i = 1, \cdots, n-1), \tag{A2}$$

$$m_n = \prod_{j=1}^{n} \bar{x}_j. \tag{A3}$$

The volume constraints are imposed on the integral of m_i, as in Eq. (6). From Eqs. (A2) and (A3), the sum of the material amounts is $\sum_{i=1}^{n} m_i = \bar{x}_1$. Therefore, the sum of the material amounts does not exceed unity. In addition, because the solid amount $\bar{x}_1$ remains unity at the interfaces between different materials, the stiffness reduction described in Section 3 does not occur.

However, extended SIMP does not have symmetry of material definition. This is shown for a case involving two materials. For two materials, Eq. (A1) becomes the following equation:

$$E = E_0 + (E_1 - E_0)\, d(\bar{x}_1) + (E_2 - E_1)\, d(\bar{x}_1)\, d(\bar{x}_2). \tag{A4}$$

$\bar{x}_1$ is the solid amount, and $\bar{x}_2$ is the fraction of the solid occupied by material 2. In the solid-filled state, $\bar{x}_1 = 1$, Eq. (A4) becomes the following equation:

$$E = E_1 + (E_2 - E_1)\, d(\bar{x}_2). \tag{A5}$$

By contrast, the linear mixture rule for the material amounts of Eqs. (A2) and (A3) is given by the following equation:

$$E_{\text{lin}} = (1 - \bar{x}_2)\, E_1 + \bar{x}_2\, E_2 = E_1 + (E_2 - E_1)\, \bar{x}_2. \tag{A6}$$

For $p \geq 1$, $d(\bar{x}_2) \leq \bar{x}_2$ holds for $0 \leq \bar{x}_2 \leq 1$. Therefore, from Eqs. (A5) and (A6), $E \leq E_{\text{lin}}$ holds when $E_2 > E_1$, and material mixing is penalized. However, when the order of material definition is swapped such that $E_2 < E_1$, $E \geq E_{\text{lin}}$ holds, and material mixing becomes advantageous. In other words, material mixing is only penalized when the stiffer material is defined later. Consequently, under extended SIMP, the optimization problem itself changes depending on the order of material definition, even for the same material combination.

Replication of results

The formulation and sensitivity analysis of the proposed scheme are described in Sections 4 to 5, and the analysis models, material properties, boundary conditions, and optimization settings are given in Sections 6 to 9. The numerical data in the figures and tables and further details about implementation are available from the corresponding author upon reasonable request.

References

[1] Bendsøe, M.P., Sigmund, O.: Material interpolation schemes in topology optimization. Archive of Applied Mechanics **69**, 635–654 (1999) https://doi.org/10.1007/s004190050248

[2] Sigmund, O., Torquato, S.: Design of materials with extreme thermal expansion using a three-phase topology optimization method. Journal of the Mechanics and Physics of Solids **45**, 1037–1067 (1997) https://doi.org/10.1016/S0022-5096(96)00114-7

[3] Gibiansky, L.V., Sigmund, O.: Multiphase composites with extremal bulk modulus. Journal of the Mechanics and Physics of Solids **48**, 461–498 (2000) https://doi.org/10.1016/S0022-5096(99)00043-5

[4] Yin, L., Ananthasuresh, G.K.: Topology optimization of compliant mechanisms with multiple materials using a peak function material interpolation scheme. Structural and Multidisciplinary Optimization **23**, 49–62 (2001) https://doi.org/10.1007/s00158-001-0165-z

[5] Zuo, W., Saitou, K.: Multi-material topology optimization using ordered SIMP interpolation. Structural and Multidisciplinary Optimization **55**, 477–491 (2017) https://doi.org/10.1007/s00158-016-1513-3

[6] da Silveira, O.A.A., Palma, L.F.: Some considerations on multi-material topology optimization using ordered SIMP. Structural and Multidisciplinary Optimization **65**, 261 (2022) https://doi.org/10.1007/s00158-022-03379-7

[7] Ding, W.: An easy-to-use univariate mapping-based method for multi-material topology optimization with implementation in MATLAB. Structural and Multidisciplinary Optimization **68**, 48 (2025) https://doi.org/10.1007/s00158-025-03983-3

[8] Liao, H., Yuan, W., Ai, S., Yuan, X.: An univariate method for multi-material topology optimization and its application to engineering structures with unstructured meshes. Computer Methods in Applied Mechanics and Engineering **437**, 117749 (2025) https://doi.org/10.1016/j.cma.2025.117749

[9] Swan, C.C., Kosaka, I.: Voigt–Reuss topology optimization for structures with linear elastic material behaviours. International Journal for Numerical Methods in Engineering **40**, 3033–3057 (1997) https://doi.org/10.1002/(SICI)1097-0207(19970830)40:16<3033::AID-NME196>3.0.CO;2-Z

[10] Tavakoli, R., Mohseni, S.M.: Alternating active-phase algorithm for multimaterial topology optimization problems: a 115-line MATLAB implementation. Structural and Multidisciplinary Optimization **49**, 621–642 (2014) https://doi.org/10.1007/s00158-013-0999-1

[11] Stegmann, J., Lund, E.: Discrete material optimization of general composite shell structures. International Journal for Numerical Methods in Engineering **62**, 2009–2027 (2005) https://doi.org/10.1002/nme.1259

[12] Noda, M., Noguchi, Y., Yamada, T.: Extended level set method: a multiphase

representation with perfect symmetric property, and its application to multi-material topology optimization. Computer Methods in Applied Mechanics and Engineering **393**, 114742 (2022) https://doi.org/10.1016/j.cma.2022.114742

[13] Sørensen, S.N., Sørensen, R., Lund, E.: DMTO—a method for discrete material and thickness optimization of laminated composite structures. Structural and Multidisciplinary Optimization **50**, 25–47 (2014) https://doi.org/10.1007/s00158-014-1047-5

[14] Lund, E.: Discrete material and thickness optimization of laminated composite structures including failure criteria. Structural and Multidisciplinary Optimization **57**, 2357–2375 (2018) https://doi.org/10.1007/s00158-017-1866-2

[15] Ogawa, S., Yonekura, K., Suzuki, K.: Multimaterial topology optimization of unsteady heat conduction problems based on discrete material optimization. International Journal of Heat and Mass Transfer **225**, 125353 (2024) https://doi.org/10.1016/j.ijheatmasstransfer.2024.125353

[16] Nam, V.T., Ogawa, S., Suzuki, K., Kawamura, Y.: Discrete material optimization approach for multi-material topology optimization of viscoelastic material for transient problem. Finite Elements in Analysis and Design **257**, 104556 (2026) https://doi.org/10.1016/j.finel.2026.104556

[17] Bruyneel, M.: SFP—a new parameterization based on shape functions for optimal material selection: application to conventional composite plies. Structural and Multidisciplinary Optimization **43**, 17–27 (2011) https://doi.org/10.1007/s00158-010-0548-0

[18] Gao, T., Zhang, W.: A mass constraint formulation for structural topology optimization with multiphase materials. International Journal for Numerical Methods in Engineering **88**, 774–796 (2011) https://doi.org/10.1002/nme.3197

[19] Yi, B., Yoon, G.H., Zheng, R., Liu, L., Li, D., Peng, X.: A unified material interpolation for topology optimization of multi-materials. Computers & Structures **282**, 107041 (2023) https://doi.org/10.1016/j.compstruc.2023.107041

[20] Hvejsel, C.F., Lund, E.: Material interpolation schemes for unified topology and multi-material optimization. Structural and Multidisciplinary Optimization **43**, 811–825 (2011) https://doi.org/10.1007/s00158-011-0625-z

[21] Kennedy, G.J., Martins, J.R.R.A.: A laminate parametrization technique for discrete ply-angle problems with manufacturing constraints. Structural and Multidisciplinary Optimization **48**, 379–393 (2013) https://doi.org/10.1007/s00158-013-0906-9

[22] Sarkar, S.I., Singh, N., Saxena, A., Kumar, P.: A generalized shape function approach for multimaterial topology optimization. International Journal for

Numerical Methods in Engineering **127**, 70401 (2026) https://doi.org/10.1002/nme.70401

[23] Zhou, Y., Nomura, T., Saitou, K.: Multi-component topology and material orientation design of composite structures (MTO-C). Computer Methods in Applied Mechanics and Engineering **342**, 438–457 (2018) https://doi.org/10.1016/j.cma.2018.07.039

[24] Chandrasekhar, A., Suresh, K.: Multi-material topology optimization using neural networks. Computer-Aided Design **136**, 103017 (2021) https://doi.org/10.1016/j.cad.2021.103017

[25] Bourdin, B.: Filters in topology optimization. International Journal for Numerical Methods in Engineering **50**, 2143–2158 (2001) https://doi.org/10.1002/nme.116

[26] Bruns, T.E., Tortorelli, D.A.: Topology optimization of non-linear elastic structures and compliant mechanisms. Computer Methods in Applied Mechanics and Engineering **190**, 3443–3459 (2001) https://doi.org/10.1016/S0045-7825(00)00278-4

[27] Wang, F., Lazarov, B.S., Sigmund, O.: On projection methods, convergence and robust formulations in topology optimization. Structural and Multidisciplinary Optimization **43**, 767–784 (2011) https://doi.org/10.1007/s00158-010-0602-y

[28] Vermaak, N., Michailidis, G., Parry, G., Estevez, R., Allaire, G., Bréchet, Y.: Material interface effects on the topology optimization of multi-phase structures using a level set method. Structural and Multidisciplinary Optimization **50**, 623–644 (2014) https://doi.org/10.1007/s00158-014-1074-2

[29] Clausen, A., Aage, N., Sigmund, O.: Topology optimization of coated structures and material interface problems. Computer Methods in Applied Mechanics and Engineering **290**, 524–541 (2015) https://doi.org/10.1016/j.cma.2015.02.011

[30] Jung, Y., Lee, J., Min, S.: Multi-material topology optimization considering joint stiffness using a two-step filtering approach. Finite Elements in Analysis and Design **197**, 103635 (2021) https://doi.org/10.1016/j.finel.2021.103635

[31] Asadpoure, A., Rahman, M.M., Nejat, S.A., Javidannia, L., Valdevit, L., Guest, J.K., Tootkaboni, M.: Topology optimization with multi-phase length-scale control. International Journal of Mechanical Sciences **291–292**, 110086 (2025) https://doi.org/10.1016/j.ijmecsci.2025.110086

[32] Guest, J.K.: Topology optimization with multiple phase projection. Computer Methods in Applied Mechanics and Engineering **199**, 123–135 (2009) https://doi.org/10.1016/j.cma.2009.09.023

[33] Wächter, A., Biegler, L.T.: On the implementation of an interior-point filter line-search algorithm for large-scale nonlinear programming. Mathematical Programming **106**, 25–57 (2006) https://doi.org/10.1007/s10107-004-0559-y

[34] Sigmund, O.: Morphology-based black and white filters for topology optimization. Structural and Multidisciplinary Optimization **33**, 401–424 (2007) https://doi.org/10.1007/s00158-006-0087-x